

Supplement of Atmos. Chem. Phys., 19, 13067–13078, 2019  
<https://doi.org/10.5194/acp-19-13067-2019-supplement>  
© Author(s) 2019. This work is distributed under  
the Creative Commons Attribution 4.0 License.



*Supplement of*

## **Lightning NO<sub>2</sub> simulation over the contiguous US and its effects on satellite NO<sub>2</sub> retrievals**

**Qindan Zhu et al.**

*Correspondence to:* Ronald C. Cohen ([rccohen@berkeley.edu](mailto:rccohen@berkeley.edu))

The copyright of individual parts of the supplement might differ from the CC BY 4.0 License.

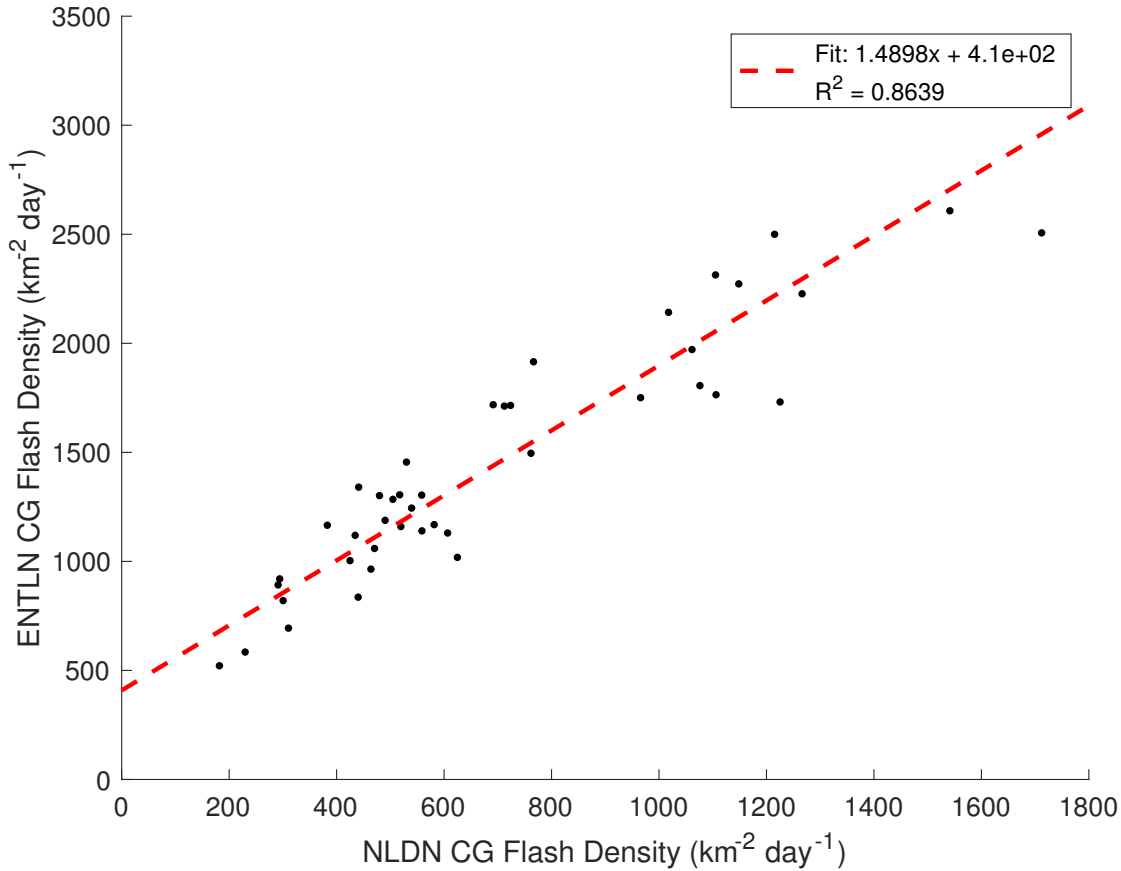


Figure S1: Comparison between CG flash density per day observed by NLDN and ENTLN. The data spans May 13 to June 23, 2012.

## S1 Comparison between ENTLN and NLDN

While both NLDN and ENTLN have high detection efficiency ( $>90\%$ ) for CG flashes, we recognize that ENTLN observes more CG flashes than NLDN. Shown in Fig. [S1](#), we average the flashes density over CONUS both from ENTLN and NLDN between May 13 to June 23 2012. The daily averaged CG flash density from ENTLN is tightly correlated with those from NLDN with slope of 1.5. It can be explained by discrepancy in the grouping criterions applied to produce flash counts between NLDN and ENTLN. ENTLN groups all pulses within 10 km and 700 ms of each other as a single flash, and NLDN uses 10 km and 1000 ms as the threshold. In consequence, for the same amount of CG pulses measured by both lightning observation network, ENTLN produces more flashes than NLDN according to the grouping algorithm.

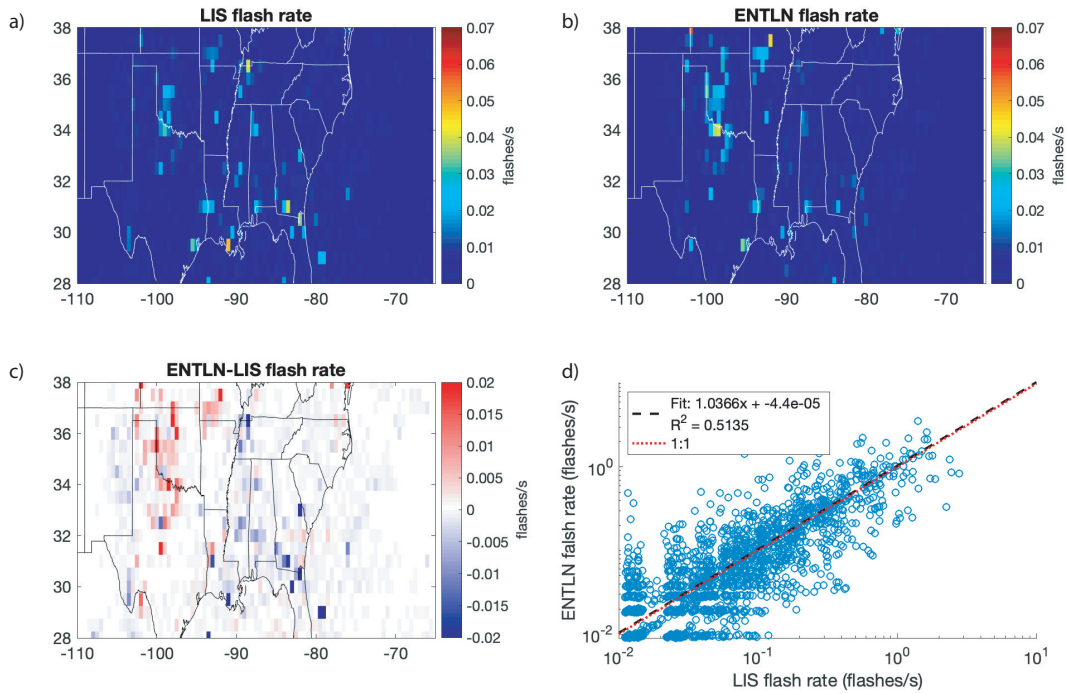


Figure S2: Comparison between flash rates observed by ENTLN and Lightning Imaging Sensor (LIS). ENTLN data is matched to corrected LIS flashes both in time and space during May 13-June 23, 2012, and both datasets are summed onto 0.5°x 0.5°grid spacing. (a,b) shows the spatial pattern of lightning flash rates measured by LIS (a) and ENTLN (b). The plot region covers 20°N - 38°N and 130°W - 65°W. (c,d) are corresponding absolute difference and scatter plots between LIS and ENTLN. LIS data is corrected using the detection efficiency from citetcecil14.

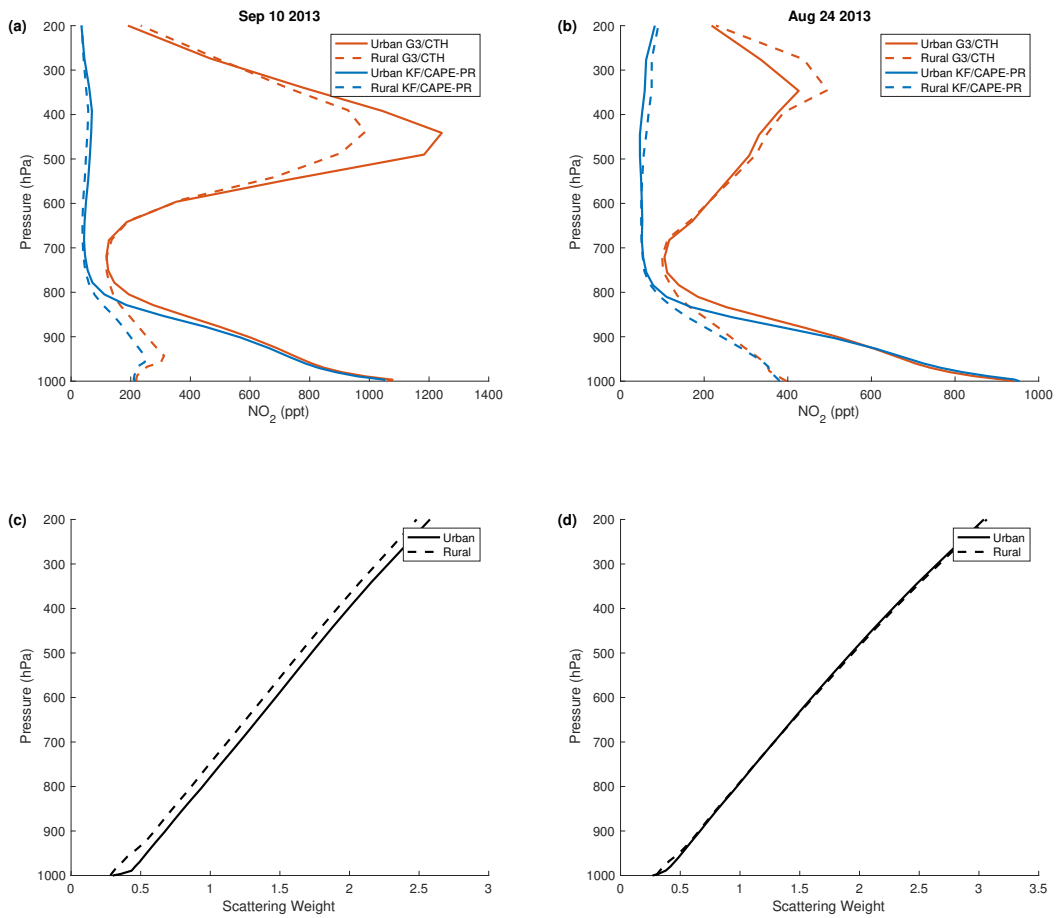


Figure S3: The a priori NO<sub>2</sub> vertical profiles (a, b) and scattering weights (c, d) on Sep 10 and Aug 24 2013 averaged over all urban (solid) or rural (dashed) grid cells in SE US. The NO<sub>2</sub> profiles from WRF-Chem using G3/CTH parameterization are in red, those from KF/CAPE-PR parameterization are in blue.

	No lightning	400 mol NO $flash^{-1}$	500 mol NO $flash^{-1}$	665 mol NO $flash^{-1}$
CONUS	$0.92 \times 10^{15}$	$0.44 \times 10^{15}$	$0.41 \times 10^{15}$	$0.44 \times 10^{15}$
Urban	$1.30 \times 10^{15}$	$0.89 \times 10^{15}$	$0.91 \times 10^{15}$	$1.10 \times 10^{15}$
Non-Urban	$0.90 \times 10^{15}$	$0.41 \times 10^{15}$	$0.37 \times 10^{15}$	$0.39 \times 10^{15}$

Table S1: The root-mean-square errors (RMSE) in unit of mole  $cm^{-2}$  between observed and modeled  $NO_2$  VCD using WRF-Chem with varied  $LNO_x$  production rates (0, 400, 500, 665 mol NO  $flash^{-1}$ ). Urban areas are selected where  $NO_2$  columns are at top 5% calculated from WRF-Chem without lightning. Non-urban areas are CONUS excluding urban areas.

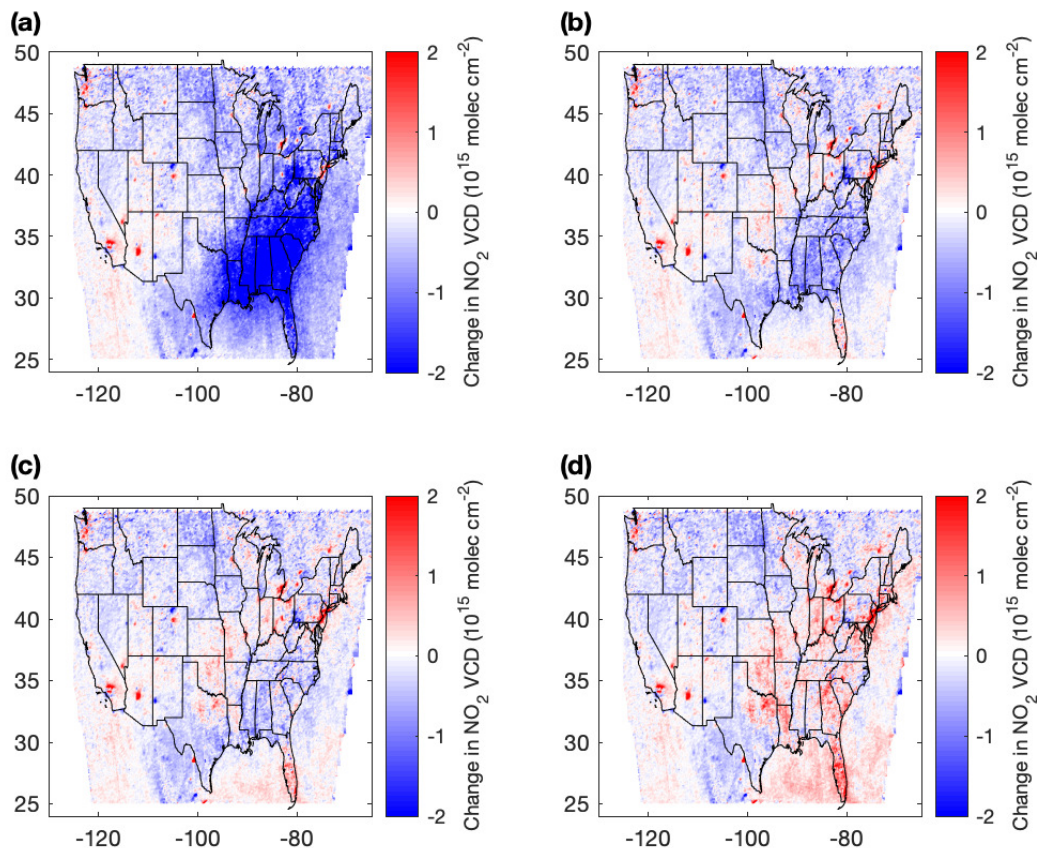


Figure S4: Difference in  $NO_2$  VCD between BEHR retrievals and WRF-Chem (a) without  $LNO_x$  and with  $LNO_x$  production rate of (b) 400 mol NO  $flash^{-1}$ , (c) 500 mol NO  $flash^{-1}$  and (d) 665 mol NO  $flash^{-1}$ .

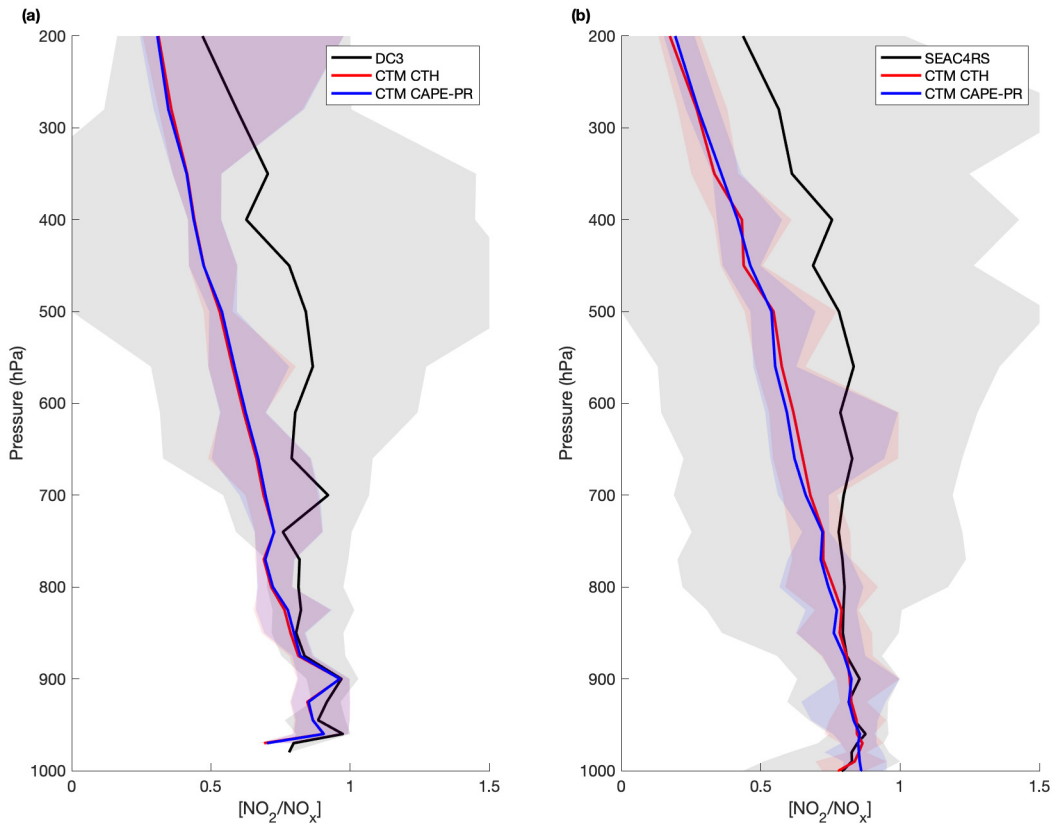


Figure S5: Comparison of WRF-Chem and aircraft  $[\text{NO}_2/\text{NO}_x]$  profiles from the (a) DC3, (b) SEAC4RS campaigns. The solid line is the median of all profiles and the shaded areas are between 10th and 90th percentiles for each binned level. Aircraft measurements are shown in black, WRF-Chem using CTH lightning parameterization in red and WRF-Chem using CAPE-PR lightning parameterization in blue.